PROCEEDINGS

Editors
Stevan Maksimović
Tomislav Igić
Nataša Trišović

Vrnjačka Banja, Serbia, June 4-7, 2013
4th International Congress of Serbian Society of Mechanics

Editors
Prof. Dr. Stevan Maksimović
Prof. Dr. Tomislav Igić
Doc. Dr. Nataša Trišović

Computer editing
Ivana Ilić, Marija Blažić, Marko Bojanić, Bojan Međo

Press
"Beotele Prom", Beograd

Circulation
200 copies

CIP

CIP - Каталогизација у публикацији
Народна библиотека Србије, Београд

531/534(082)

SERBIAN Society of Mechanics (Beograd). International Congress (4 ; 2013 ; Vrnjačka Banja)

Proceedings / 4th International Congress of Serbian Society of Mechanics, 4-7th June, 2013, Vrnjačka Banja ; editors Stevan Maksimović, Tomislav Igić and Nataša Trišović. - Belgrade : Serbian Society of Mechanics, 2013 (Beograd : Beotele Prom). - XXIV, 1010 str. : ilustr. ; 25 cm

Tiraž 200. - Str. III: Preface / S. [Stevan] Maksimović & T. [Tomislav] Igić. - Registar. - Bibliografija uz svaki rad.

ISBN 978-86-909973-5-0

a) Механика – Зборници

COBISS.SR-ID 198308876

Published by Serbian Society of Mechanics, Belgrade
http://www.ssm.org.rs/

PREFACE

These proceedings contains the papers presented at the Forth (29th Yu) International Congress of Serbian Society of Mechanics held in Vrnjačka Banja during the period 4th – 7th June, 2013.

Theoretical and Applied Mechanics is a subject of great importance in the developing of science and technology. The aim of the Congress is to provide a forum to exhibit the progress in this field during the past years and a place to further the interaction between of modern theoretical and applied mechanics, as well as modern engineering sciences.

The papers, contributed by authors from all around the globe, have been separated into 7 sections which cover the main areas of interest: `Plenary Lectures`, Section A, Section B, Section C, Section D and two Mini-symposia.

We would like to express our gratitude to all members of the Scientific Committee and also to the participants for their engagement in organizing of the Congress, including the preparation of manuscripts to be published in the Journal Theoretical and Applied Mechanics, Scientific Technical Review and Journal of Serbian Society for Computational Mechanics.

It gives us great pleasure to express our deep appreciation for the great long-standing support that Prof. Dr. Nikola Hajdin, President of the Serbian Academy of Sciences and Arts, has given to the promotion of all aspects of theoretical and applied mechanics in Serbia.

Last, the Congress organizing committee wishes to acknowledge the collaboration of the Ministry of Education, Science and Technological Development of the Republic of Serbia, Serbian Academy of Sciences and Arts, Municipality Vrnjačka Banja and many supporting members of the Serbian Society of Mechanics.

S. MAKSIMOVIĆ & T. IGIĆ
June, 2013

Scientific Committee

Nikola Hajdin (Belgrade, Serbia)
Miloš Kojić (Kragujevac, Serbia)
Vladan Đorđević (Belgrade, Serbia),
Božidar Vujanović (Novi Sad, Serbia)
Đorđe Zloković (Belgrade, Serbia)
Felix Chernousko (Moscow, Russia)
Antony Kounadis (Ethens, Greece)
Ingo Müller (Berlin, Germany)
Đorđe Đukić (Novi Sad, Serbia)
Teodor Atanacković (Novi Sad, Serbia)
Ardeshir Guran (Ontario, Canada)
Ranislav Bulatović (Podgorica, Montenegro)
Vlado Lubarda (San Diego, CA, USA)
Katica (Stevanović) Hedrih (Niš, Serbia)
Anatoly M. Samoilenko (Kiev, Ukraine)
Emanuel Gdoutos (Patras, Greece)
Hiroshi Yabuno (Tokiyo, Japan)
John Katsikadelis (Ethens, Greece)
M.P.Cartmell (Glasgow, Scotland, UK)
Giuseppe Rega (Roma, Italy)
Jan Awrejcewicz (Lodz, Poland)
J. M. Balthazar (Sao Paolo, Brazil)
J. A. Tenreiro Machado (Porto, Portugal)
Pauel Kraseilnikov (Moscow, Russia)
Subhash C. Sinha (Auburn, Alabama)
Jerzy Warminski (Lublin, Poland)
Yuri Mikhilin (Kharkov, Ukraine)
Vesna Milošević-Mitić (Belgrade, Serbia)
Jovo Jarić (Belgrade, Serbia)
Bohdana Marvalova (Czech Republic)
Alexander Seyranin (Moscow, Russia)
Chi Chow (Michigen, United States)
Lidia Kurpa (Khrakov, Ukraine)
Treinhold Kienzler (Bremen, Germany)
Marina Shitikova (Russia)
RadeVignjević (Cranfield, England)
Andrea Carpinteri (Parma, Italy)
Vlada Đurković (Belgrade, Serbia)
Slobodan Stupar (Belgrade, Serbia)
Miloš Nedeljković (Belgrade, Serbia)
Milorad Milovančević (Belgrade, Serbia)
Zoran Rajić (Belgrade, Serbia)
Nikola Mladenović (Belgrade, Serbia)
Aleksandar Obradović (Belgrade, Serbia)
Mihailo Lazarević (Belgrade, Serbia)
Tamara Nestorović (Bohum, Germany)
Strain Posavljak (Banja Luka, Republic of Srpska)
Livija Cvetićanin (Novi Sad, Serbia)
Ivana Kovačić (Novi Sad, Serbia)
Milan Mićunović (Kragujevac, Serbia)
Dragan Milosavljević (Kragujevac, Serbia)
Miroslav Živković (Kragujevac, Serbia)
Nenad Filipović (Kragujevac, Serbia)
Vladimir Dragović (Belgrade, Serbia)
Slobodanka Boljanović (Belgrade, Serbia)
Vladimir Raičević (Kosovska Mitrovica, Serbia)
Zoran Mitrović (Belgrade,Serbia)
Predrag Kozić (Niš, Serbia)
Ratko Pavlović (Niš, Serbia)
Dragoslav Kuzmanović (Belgrade, Serbia)
Dragoslav Šumarac (Belgrade, Serbia)
Petar Mitković (Niš, Serbia)
Vlastimir Nikolić (Niš, Serbia)
Taško Maneski (Belgrade, Serbia)
Borislav Gajić (Belgrade, Serbia)
Dragan Spasić (Novi Sad, Serbia)
Marina Kutin (Belgrade, Serbia)
Ljubica Milović (Belgrade, Serbia)
Marko Rakin (Belgrade, Serbia)
Aleksandar Sedmak (Belgrade,Serbia)
Dušan Najdanović (Belgrade, Serbia)
Milomir Gašić (Kraljevo, Srbija)
Boško Rašuo (Belgrade, Serbia)
Pol Spanos (Houston, TX, USA)
NatašaTrišović (Belgrade, Serbia)
Tomislav Igić (Niš, Serbia)
Stevan Maksimović (Belgrade, Serbia)

Organizing Committee

Stevan Maksimović (Chairman) VTI-Aeronautical Department, Belgrade, Serbia
Tomislav Igić (Chairman) Faculty of Civil Engineering, Niš, Serbia
Nataša Trišović (Secretary) Faculty of Mechanical Engineering, Belgrade, Serbia
Bojan Međo, Faculty of Technology and Metallurgy, Belgrade, Serbia
Ivana Ilić, VTI-Aeronautical Department, Belgrade, Serbia
Ivana Vasović, GOŠA Institute, Belgrade, Serbia
Marija Blažić, VTI-Aeronautical Department, Belgrade, Serbia
Marko Bojanić, VTI-Aeronautical Department, Belgrade, Serbia

Table of Contents

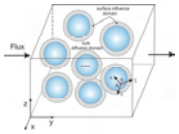

Plenary lectures

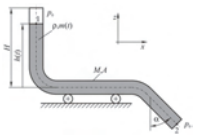

Section A: General Mechanics

Section B: Fluid Mechanics

COMPARISON OF NUMERICAL AND SCALE MODELS OF STEPPED SPILLWAY FLOW

Budo Zindović[1], Ljubodrag Savić[2], Radomir Kapor[3], Nikola Mladenović[4]

[1] Faculty of Civil Engineering, University of Belgrade, Serbia
e-mail: bzindovic@hikom.grf.bg.ac.rs
[2] Faculty of Civil Engineering, University of Belgrade, Serbia
e-mail: ljdsavic@grf.bg.ac.rs
[3] Faculty of Civil Engineering, University of Belgrade, Serbia
e-mail: rkapor@hikom.grf.bg.ac.rs
[4] Faculty of Mechanical Engineering,
The University of Belgrade, Kraljice Marije 16, 11120 Belgrade 35
e-mail: nmladenovic@mas.bg.ac.rs

Abstract. This paper deals with flow modelling of the stepped spillway for the Bogovina dam. The analysis was conducted using three approaches: scale-modelling, empirical equations and numerical modelling. An acceptable agreement was achieved between the empirical equations and the numerical model results, while both of them exhibit considerable differences when compared to scale-model. These discrepancies can be contributed to the difficulties in modeling the process of air-entrainment. Since air-entrainment is important for providing good estimates, existing empirical equations as well as numerical models require further improvements.

1. Introduction

In the last three decades, stepped spillways have become common overflow structures for roller-compacted concrete (RCC) dams. The steps have significant influence on the energy dissipation along the spillway and reduce the size and the cost of the stilling basin. The application of new construction technique of roller-compacted concrete, had lowered the construction cost even more. Low cost, combined with good energy dissipation make RCC dams a superior alternative to traditional concrete gravity dams with smooth spillways.

Hydraulic characteristics of stepped spillways can be assessed in various ways: by using the empirical equations (during the preliminary design process), scale modeling, and numerical modeling (in the final design process). These three approaches are applied to the spillway of the 'Bogovina' dam.

RCC dam 'Bogovina' is planned to impound the water of the Timok River. Proposed height of the dam is 54 m, with crest width of 396 m. The design flow of the spillway is $Q_{0,01\%} = 372$ m^3/s and the width is 115 m. The spillway is inclined $\phi = 51{,}34^o$ with respect to horizontal plane. Proposed height of the first four steps is 45 cm, while the remaining 45 steps are 90 cm. The downstream end of the spillway is connected to the stilling basin.

2. Materials and methods

2.1. Scale model

In order to obtain valid data for the analyses, the scale of the model should be chosen so that the flow can exhibit adequate air entrainment. To comply with this requirement, it is sufficient to use scales between 1:10 to 1:12. Since the large spillway discharge of the Bogovina dam, and importance of correct air entrainment modeling for representative energy dissipation, it was chosen to build only a section of the weir with stepped spillway (Figure 1) [3, 4]. Scale of such model was 1:12 with respect to Froude similitude. Width of this model was 60 cm. Water levels in the spillway were measured with point gauges.

Figure 1. Scale model of the section of the weir with the stepped spillway of the Bogovina dam [3, 4]

2.2. Empirical equations for the stepped spillways

Boes and Hager [1, 2] conducted a series of tests on scale models, and devised equations for the analysis of the stepped spillways flow. In the remaining part of this section, an overview of this analysis is presented. The details are outlined in the literature [3].

Inception point. Inception point is the location where boundary layer intersects the free surface downstream of the weir. Downstream of this location a significant air entrainment occurs.

Uniform flow characteristics. If the spillway chute is long enough, the flow is expected to attain uniform conditions. Since this type of flow is positioned downstream of inception point, it will exhibit a significant air entrainment. One can distinguish between the clear-water depth, and the mixture depth, where the concentration of entrained air is 90%.

Residual energy along the spillway chute. Residual energy per unit weight of the water is an important parameter for designing the stilling basin. As the cost of the basin can be

significant, it is essential to provide a reasonably good estimate of the residual energy at the downstream end of the spillway.

2.3. Numerical modeling of the flow along the spillway

For numerical modelling of the flow field along the stepped spillway, software package Ansys Fluent v14 has been selected. As the process of an air-entrainment is crucial for the problem, a two-phase model was used. Water and air were considered as separate interpenetrating continua. Mass and momentum conservation equations are solved for each phase, q [5]:

$$\frac{\partial}{\partial t}\left(\alpha_q \rho_q\right) + \frac{\partial}{\partial x_k}\left(\alpha_q \rho_q u_q^k\right) = 0 \ , \tag{1}$$

$$\frac{\partial}{\partial t}\left(\alpha_q \rho_q u_q^i\right) + \frac{\partial}{\partial x_j}\left(\alpha_q \rho_q u_q^j u_q^i\right) = \alpha_q \rho_q g^i - \alpha_q \frac{\partial p}{\partial x_i} + \frac{\partial \tau_q^{ij}}{\partial x_j} + F_q^i \ , \tag{2}$$

where α_q – fraction of the phase q in the control volume, ρ_q – density of the phase q, u_q^i – velocity component of phase q in the x_i direction , g^j – gravity acceleration vector, p – pressure, τ_q^{ij} – shear stress tensor (viscous and turbulent) for the phase q, and F_q^i – force term, accounting for the interaction between phases (lift, virtual mass). Vectors and tensors are written in tensor notation, and each component in the Cartesian direction x_i is denoted by the upper index, i.

The turbulence was described with Reynolds stress model for each component [5]:

$$\frac{\partial}{\partial t}\left(\alpha_q \rho_q R_q^{ij}\right) + \frac{\partial}{\partial x_k}\left(\alpha_q \rho_q u_q^k R_q^{ij}\right) = D_q^{ij} + P_q^{ij} + \phi_q^{ij} + \varepsilon_q^{ij} \, , \tag{3}$$

where R^{ij} is the "Reynolds stress tensor", D^{ij} – diffusion tensor (molecular and turbulent), P^{ij} – Reynolds stress production tensor, ϕ^{ij} – pressure strain tensor, and ε^{ij} the dissipation tensor.

The process of air dissolving was not modeled, as insignificant for the given problem.

The system of eqs. (1) – (3) for both (q) phases is solved by supplying appropriate boundary conditions. For Equation (1), one must prescribe phase distribution while the Equations (2) require the velocity distribution for all boundaries.

3. Results and discussion

In this section, the results from the scale model, empirical equations [3] and numerical model are compared for the water flow of $Q = 372$ m^3/s. The results are summarized in Table 1.

Table 1. Summary of the results from the scale-model, empirical equations and numerical model for the Bogovina dam stepped spillway. All values are up-scaled to the prototype dam: L_i – inception point distance, $h_{90,u}$ – uniform flow mixture depth, $\overline{C}_u$ – averaged air concentration for uniform flow, $h_{90,11}$ and $h_{90,16}$ – mixture depths at steps 11 and 16, H_{RES} – residual energy at step 16.

	Scale-model	Empirical eqs.	Fluent
L_i [m]	7,12	8,74	8,9
$h_{90,u}$ [m]	0,72	0,55	0,52
$\overline{C}_u$ [-]	-	0,55	0,22
$h_{90,11}$ [m]	0,56	0,61	0,51
$h_{90,16}$ [m]	0,72	0,62	0,52
H_{RES} [m]	-	8,12	4,4

The inception point. As seen from Table 1, length from the weir crest to the inception point is the smallest for the scale-model. The location computed from empirical equations and numerical model are in good agreement with each other, and are somewhat larger than the measured.

Uniform flow mixture depths and air concentrations. The uniform flow mixture depths computed from empirical equations and numerical model show good agreement, but both of them are smaller than the measured. This could come from the fact that the uniform depth might not have been attained at the scale model.

As the concentration of the entrained air was not measured, comparison was made only between the results of the empirical equations and the numerical model. The difference between them is significant (2.5 times).

Mixture depths at the steps 11 and 16. The measured mixture depths and the depths obtained with the empirical equations are larger than the depths from the numerical model. The disagreements at the step 11 are within acceptable limits, which cannot be observed for the step 16. From the analysis presented in [3], the flow is expected to attain the uniform condition between the steps 11 and 16. As the depths obtained from the numerical model in the respective sections are similar, one can conclude that the uniform flow occurs further upstream than expected in the numerical model. Aside from the overall flow structure, it is important to consider the flow field within the triangular cavities formed by the steps. The numerical model flow field exhibits the swirls inside the cavity, which was also observed in the scale model (see Figure 3). This flow pattern is visualized by the streamlines in the numerical model and the entrained air in the scale model photo. Also, it is noted that the numerical model is able to reproduce air-water mixture only to a certain extent, in the region close to the free surface. However, the model isn't able to reproduce the air entraining in the cavity itself.

Residual energy head. Residual energy head (residual energy per unit weight of water) was analyzed using the empirical equations and numerical model only. The residual energy head obtained from the numerical model is ≈50% of the value computed by the empirical equations. The reason for the difference could be the discrepancy of air concentration. As shown in [1, 2], the friction factor decreases with air concentration. As stated previously, the air concentrations from the numerical model are smaller than expected (empirical equations), which results in larger friction factor and larger energy dissipation. Since the reliable prediction of energy dissipation is of crucial importance for a stilling basin design, it is necessary to conduct further research in order to obtain an accurate prediction of the residual energy.

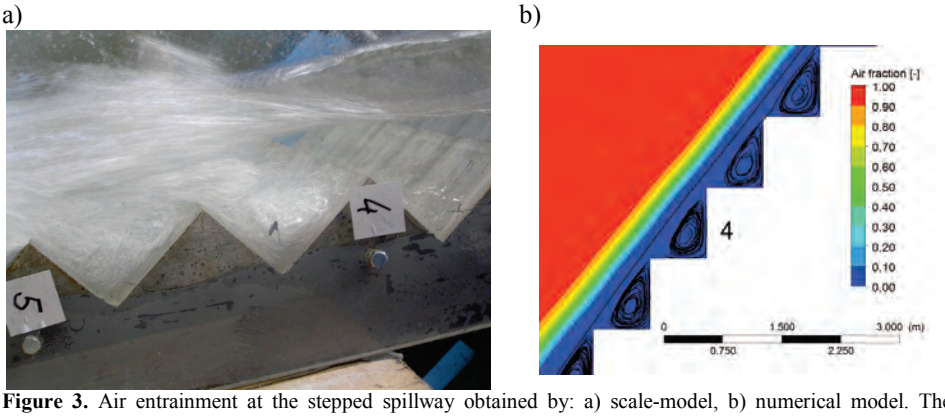

Figure 3. Air entrainment at the stepped spillway obtained by: a) scale-model, b) numerical model. The recirculating flow in the triangular cavity, formed by the steps, was observed on the scale model as well as the air entrained in the cavity. The numerical model was able to reproduce the recirculating flow pattern in the cavity (see the streamlines). Modeling of air water mixing was restricted to the free surface zone, but was not reproduced within the cavity itself.

4. Conclusions

The comparison between the results of the scale-model, empirical equations, and numerical model Ansys Fluent for the Bogovina dam are presented. The following can be concluded:

- Location of the inception point is obtained with acceptable agreement for all three approaches.
- Uniform flow mixture depths by the numerical model are predicted upstream from the position expected by the empirical equations.
- Entrained air concentration for the uniform flow conditions is significantly underestimated by the numerical model.
- Although the flow field over the steppes is well reproduced, the numerical model failed to simulate the air entrainment process inside the triangular cavity formed by the steps.
- Residual energy is significantly underestimated by the numerical model, which is not on the safe side for stilling basin design.

- In order to provide good estimates for design purposes of the stepped spillways, the existing empirical equations and the numerical model require further improvements.

Acknowledgement. Authors acknowledge the financial support through the projects TR37009 and TR 35043, funded by the Serbian Ministry of Education, Science and Technological Development.

References

[1] Boes, R M and Hager W H (2003a), Two-Phased Flow Characteristics of Stepped Spillways, *Journal of Hydraulic Engineering*, **129**, pp. 661–670.
[2] Boes, R M and Hager W H (2003b), Two-Phased Flow Characteristics of Stepped Spillways, *Journal of Hydraulic Engineering*, **129**, pp. 671–679.
[3] Kapor R, Savić Lj, Žugić D, Petrović N, Rula M (2006) Comparison of computed and scale model results of stepped spillways, *Proceedings of the 14th Conference of Serbian Association of Hydraulic Research*, Fruška Gora, pp. 105-117. (videti ostale podatke)
[4] Žugić D, Kapor R, Pop Trajković V, Petrović N, Rula M, (2006) Scale modeling of stepped spillway in two different scales, *Proceedings of the 14th Conference of Serbian Association of Hydraulic Research*, Fruška Gora, pp. 19–28.
[5] ANSYS® Academic Research, Release 14.0, Help System, ANSYS Fluent Theory Guide, ANSYS, Inc.

SUPERCRITICAL FLOW IN CIRCULAR CLOSED-CONDUIT BENDS

Milena Kolarević[1], Ljubodrag Savić[2], Radomir Kapor[3], Nikola Mladenović[4]

[1] Energoprojekt – Hidroinženjering,
Bul. Mihaila Pupina 12, 11070 Belgrade,
milenakolarevic@yahoo.com
[2] University of Belgrade– Faculty of Civil Engineering,
Bul. kralja Aleksandra 73, 11000 Belgrade,
ljdsavic@grf.bg.ac.rs
[3] University of Belgrade– Faculty of Civil Engineering,
Bul. kralja Aleksandra 73, 11000 Belgrade
rkapor@hikom.grf.bg.ac.rs
[4] University of Belgrade – Faculty of Mechanical Engineering,
Kraljice Marije 16, 11120 Belgrade,
nmladenovic@mas.bg.ac.rs

Abstract. In this paper complex flow pattern occurring in a closed conduit bend with supercritical flow is analyzed. The research was done by a scale (physical hydraulic) model, and a numerical model developed in Ansys (Fluent) program surrounding. This article compares the results obtained by numerical and physical (scale) models, providing comments and recommendations for their application. Based on these results, simple empirical relationships were developed, describing the effects of the bend curvature, bend deflection angle and approach flow conditions (non dimensional depth and the Froude number upstream from the bend) on the considered flow.
Keywords: supercritical flow, horizontal bend, closed conduit, scale model, numerical model

1 Introduction

Supercritical flow in a circular conduit with the horizontal-plane direction change causes abrupt depth and velocity perturbations, spreading downstream in a form of standing waves. At the beginning of the bend, a positive wave is developed along the outer bend wall (concave), and a negative wave along the inner wall (convex).

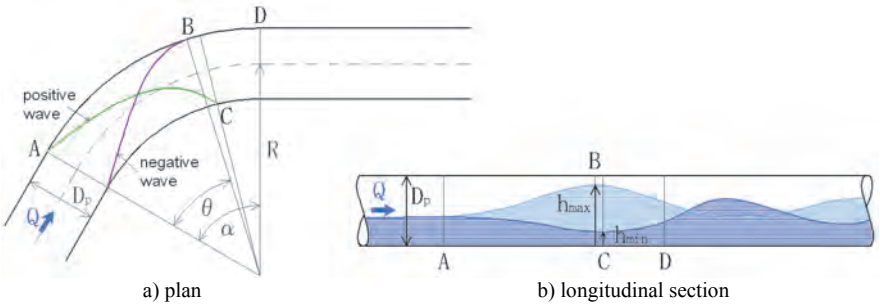

a) plan b) longitudinal section

Figure 1. Propagation of positive and negative waves along the conduit

Free surface flow in a circular bend may convert into helicoidally flow, or into pressurized (choking) flow. This article compares the results obtained by hydraulic scale (physical) and numerical model, providing comments and recommendations for their application. The hydraulic scale model was built at the laboratory of Faculty of Civil Engineering in Belgrade. Hydraulic features of the bend flow were examined by the scale model investigations, in terms of: the deflection angle, the bend curvature, and the approach flow conditions, described through: non dimensional depth, h_0/D, and Froude number, $F_{R0} = v/\sqrt{gh}$. Based on the results of the scale model investigations, simple empirical relationships were developed, describing influence of the before mentioned parameters. Also, the results from the scale model were used for calibration of the numerical model.

2 Hydraulic scale model investigations

Experimental installation consists of (fig. 2.):

- The upstream reservoir, providing controlled inflow to the conduit
- The conduit (inner diameter D=15 cm) with horizontal bend and upstream and downstream straight reaches

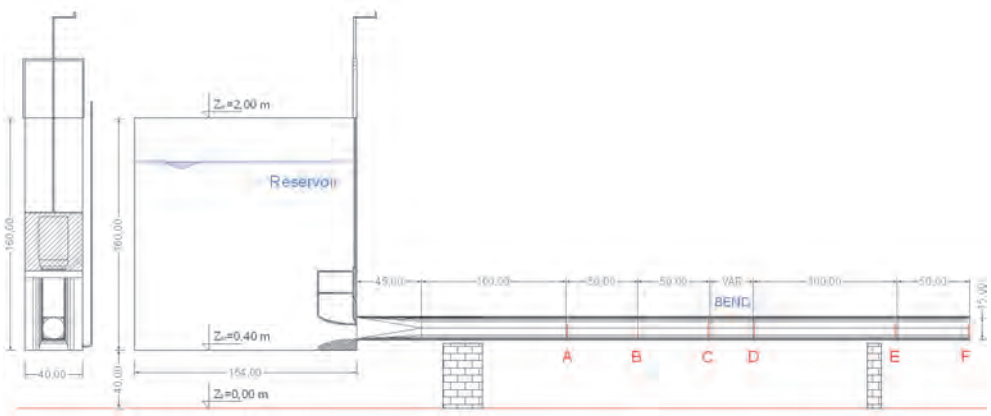

Figure 2. Longitudinal section of experimental installation

The conduit is horizontal, and the flow is steady. The length of a transition reach from squared to circular cross-section is 45 cm (3D). The length of the straight upstream reach is 245 cm, while the downstream reach is 150 cm. The inlet is hydraulically shaped to provide minimal disturbances in an approach flow. The inlet velocity is controlled by a gate. The approach flow conditions are set by changing the gate opening and the water depth in the reservoir. Water flow is measured upstream from the reservoir.
The hydraulic experiments were conducted for the bend curvatures of D/R = 1/2; 1/3; 1/4 and the deflection angles of 15°, 30°, 45° и 60°. Also, deflection angles of 75° and 90° were studied with curvature of D/R = 1/3, giving the total of 14 setups.

2.1 Analyses of experimental investigations

The Flow in the hydraulic scale model is classified in one of the four categories (Fig. 3.)

1) Flow *without turning of the jet* around the conduit axes – *stratified flow*,
2) Transition flow, with *partially turning* of the jet,
3) *Helicoidal flow*, with flow complete turning around the conduit axes (without choking),
4) Helicoidal flow with choking – *choking flow*.

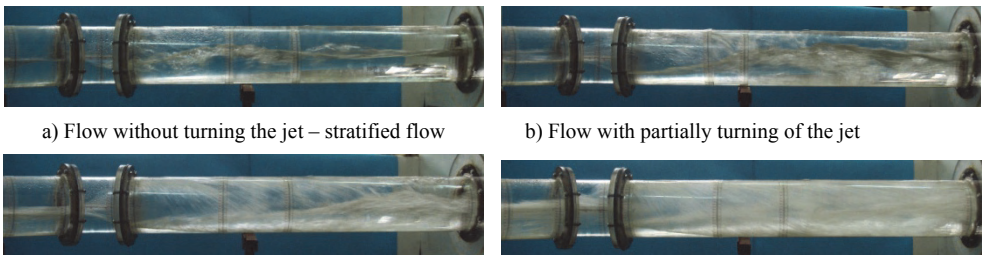

a) Flow without turning the jet – stratified flow b) Flow with partially turning of the jet

c) Helicoidal flow without choking d) Helicoidal flow with choking – chocking flow

Figure 3. Characteristic flow patterns in circular conduit bend.

This research included 182 experiments on the hydraulic scale model, with 14 setups. Non dimensional approach depth, h_0/D, varied between 0,23÷0,84, while the range of approach Froude numbers was $F_{R0} = v/\sqrt{gh}$ =1,5÷4,5. For each setup, the threshold condition for establishing of helicoidally flow and choking flow was determined.

The influence of the deflection angle on the type of flow. Fig. 4 shows the limit between stratified and helicoidally flow, depending on h_0/D and F_{R0}, for considered deflection angles and D/R = 1/3. In the table within the figure, empirical relationships, defining the curves for angles of 15° and 30° are presented, while the single relationship is valid for angles of 45°, 60°, 75° and 90°. Also is shown the empirical relationship for angle of 45°, according to [1]. All the curves proposed by the authors are above the curve from [1], suggesting that this curve is on the safe side. Fig. 4. shows that the value of deflection angle has insignificant influence on the transition to helicoidal flow for angles greater than 30°. Almost all analyzed cases for deflection angles between 45°÷90° revealed that the jet turns around the bend contour in the first 40°. The longitudinal free-surface slope along the concave bend wall does not depend on the deflection angle, but only on the bend curvature and the approach velocity. Therefore, transition to helicoidal flow is the same for the range of deflection angles between 45° and 90°. The experiments with the angle of 15° demonstrate that, in almost all the cases with helicoidal flow, the jet turns within the downstream straight reach of the conduit. The longitudinal free surface slope becomes mild when the jet leaves the bend. Hence, the jet turns around the conduit axis further downstream, than for the larger deflection angles; or it does not turn at all.

Figure 5. shows the choking flow limit, as a function on h_0/D and F_{R0}, for considered deflection angles, with D/R=1/3, together with the corresponding empirical relationships. Reduction of the deflection angle, shifts the limit of choking to higher value

h_0/D and F_{R0}. Therefore, under the same approach flow conditions, choking will occur for higher values of deflection angle.

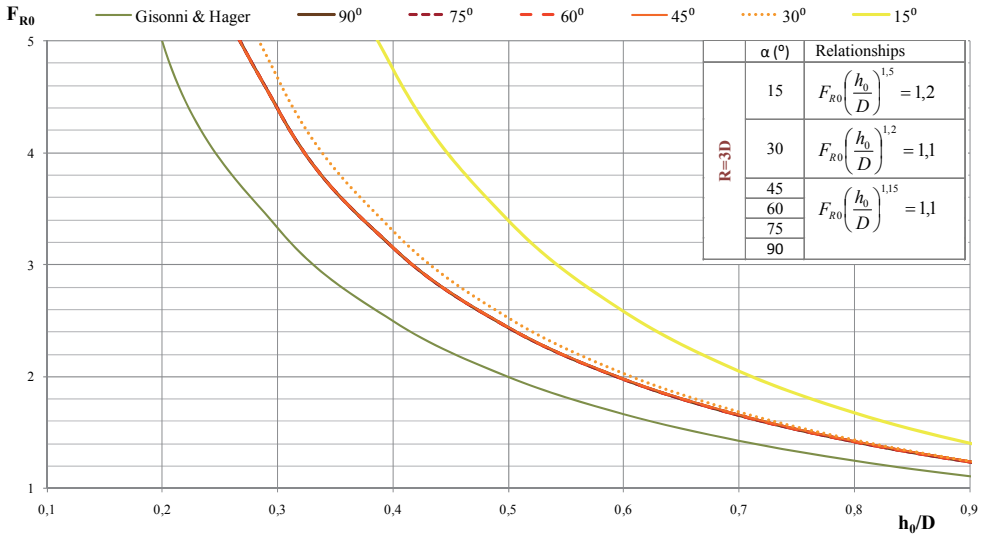

Figure 4. Limits between stratified and helicoidal flow for considered deflection angles and D/R = 1/3

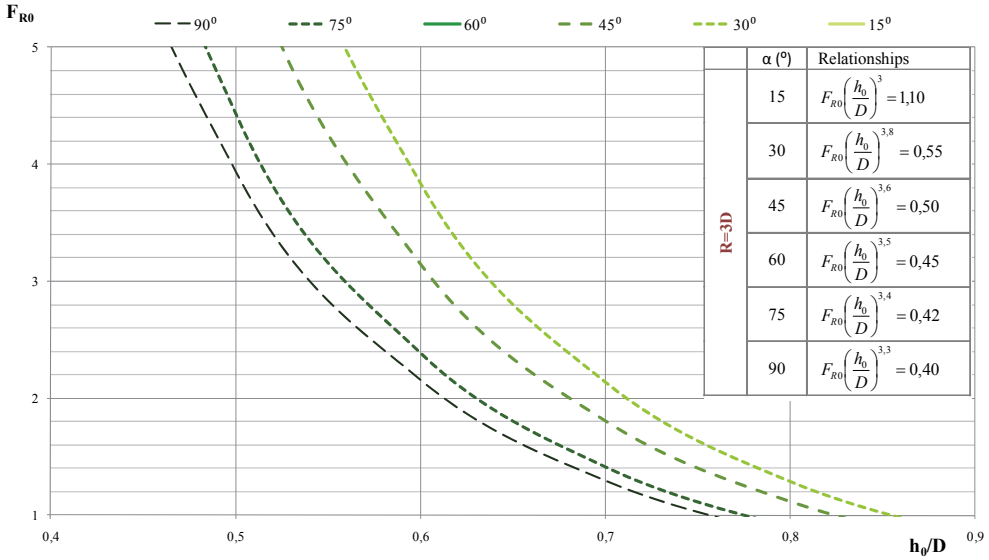

Figure 5. Limits of choking for considered deflection angles and D/R = 1/3

The influence of curvature on the type of flow. Figure 6. shows the limit between stratified and helicoidal flow, depending on h_0/D and F_{R0}, for the considered bend curvatures and the deflection angle of 45°, with corresponding empirical relationships. Also, empirical relationship for curvature of D/R = 1/3, according to [1], is presented. One can observe that

the reduction of the curvature, shifts the limit of choking to higher values of $F_{R0.}$ All the curves are above recommended curve [1], and its use is on the safe side.

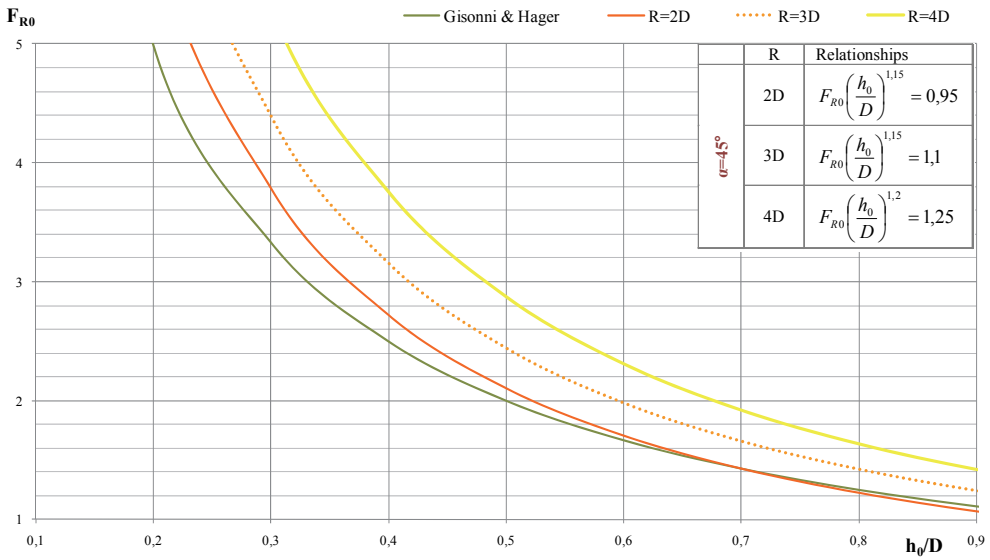

Figure 6. Limits between stratified and helicoidal flow for considered curvatures D/R and deflection angle 45°

A similar diagram presents the threshold of choking flow for the considered bend curvatures, with the deflection angle of 45° (Fig. 7).

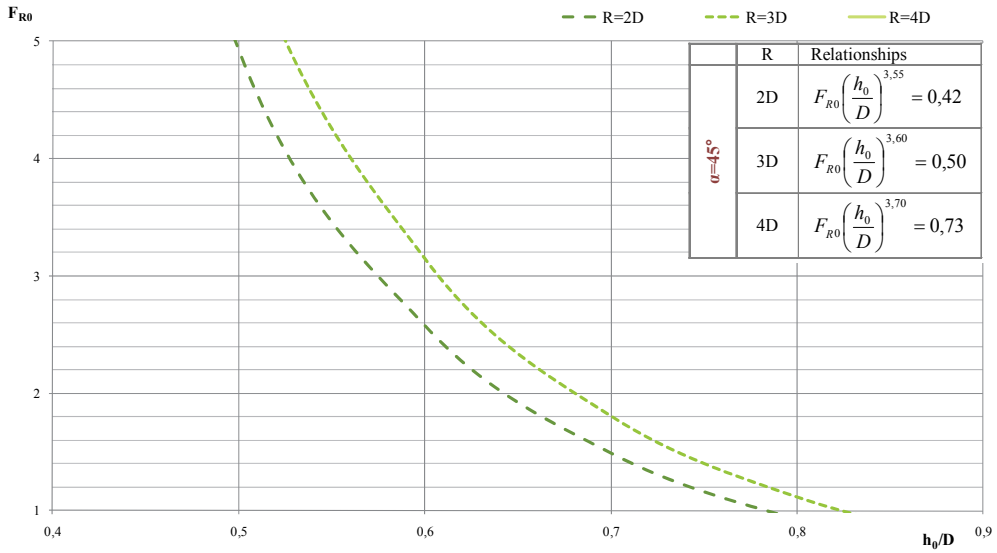

Figure 7. Limits of choking for considered curvatures and deflection angle 45°

The mutual position of the curves is similar to the case of the transition from stratified to helicoidal flow, with the same conclusions applied.

3 Numerical model and comparison to the results by the scale model

The numerical model is based on partial differential equations for the spatial flow of water and air. Model is developed in Fluent (Ansys-Fluid Dynamic) program surrounding, which uses the finite volume method. The computation domain consists of 1.330.724 hexagonal elements. The computational grid is denser in the bend region and downstream of it, and in the vicinity of the contour. The water level and the mass flow rate of water and air were prescribed at the upstream end of the conduit, while the free outflow is imposed at the downstream end.
Comparison of the results obtained by the scale and numerical models, for helicoidal flow without choking, and deflection angle of 45 ° and curvature D / R = 1/3, is presented at Fig. 8. Helicoidal flow occurred for the water flow of 22,4 l/s and approach flow depth of 9,1 cm.

a) The hydraulic scale model

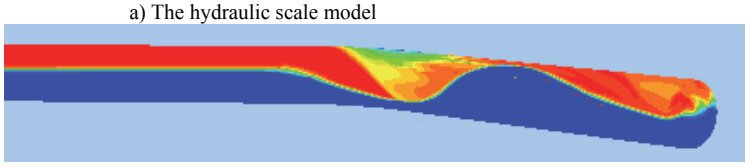

b) Numerical model

Figure 8. Comparison of hydraulic scale model and numerical model: Helicoidal flow in the conduit

One can observe a good agreement between the observed (scale model) and computed (numerical model) flow field.

4 Conclusions

Based on the hydraulic scale model experiments, empirical relationships for threshold of helicoidal and choking flow in a circular conduit bend with free surface flow, were developed. The relationships are given as functions of non dimensional approach depth, h_0/D, and approach Froude number, for considered deflection angles and bend curvatures.

A comparison of the results obtained by the scale and the numerical model, showed satisfactory agreement.

Acknowledgement. This work was supported by the Ministry of Education and Science of the Republic of Serbia under project no. TR 37009 “Monitoring and Modeling of Rivers and Reservoirs – Physical, Chemical, Biological and Morphodynamic Parameters”, and project no. TR 35043.

References

[1] Gisonni, C., Hager, W., H., (2000), *Bend Flow in Bottom Outlets,* from the Internet

THERMAL BEHAVIOUR AND TRANSVERSAL JOINT DISTANCE COMPUTATION FOR GRAVITY RCC DAMS

Vladan Kuzmanovic[1], Ljubodrag Savić[2], Nikola Mladenović[3]

[1] Faculty of Civil Engineering,
The University of Belgrade, Bul. Kralja Aleksandra 73, 11000 Belgrade
e-mail: vladak@grf.bg.ac.rs
[2] Faculty of Civil Engineering,
The University of Belgrade, Bul. Kralja Aleksandra 73, 11000 Belgrade
e-mail: ljdsavic@grf.bg.ac.rs
[3] Faculty of Mechanical Engineering,
The University of Belgrade, Kraljice Marije 16, 11120 Belgrade
e-mail: nmladenovic@mas.bg.ac.rs

Abstract. Roller Compacted Concrete (RCC) is a special concrete mixture with low cement content, frequently used for concrete gravity dams. This paper deals with the 3D finite element model for unsteady phased thermal-stress analysis of RCC dams. Model calibration and verification has been done, based on the in-situ measurements of the Platanovryssi dam. The study has been done using the actual dam shape, RCC time schedule, and material properties. The results proves that the recommended 3D model enables a reliable thermal-stress prediction and transversal joint distance computation for an RCC gravity dam.

Keywords: RCC dam, thermal analysis, thermal stress, transversal joint distance

1. Introduction

Roller Compacted Concrete (RCC) is a special concrete mixture with low cement content, frequently used for concrete gravity dams. To reduce the thermal cracking, RCC dams are usually cut by transverse contraction joints into monoliths. The number and position of the joints should be determined based on the thermal-stress computations. The numerical model should consist of: (a) definition of the thermal and mechanical RCC properties, (b) computation of the temporal evolution of the thermal field, and (c) thermal-stress computation. Up to date models do not simulate accurately the long-term RCC behaviour ([1], [2]), due to simplifications. This research presents one of the first attempts to faithfully predict the RCC dams contraction joint distance, and to estimate it's influence on the thermal stress field. The developed model takes into account: the actual shape of the dam, different types of concrete, actual initial and boundary conditions, thermal and mechanical properties of RCC and construction technology, [3]. Calibration and verification are based on the in-situ measurements of the Platanovryssi dam, [4].

2. Theoretical background

The change of temperature (T) of a nonhomogeneous, isotropic body in time (t), due to the hydration heat, is described by the Fourier heat conductivity equation. If the thermal conductivity is independent of space and temperature:

$$\frac{\partial \mathrm{T}}{\partial \mathrm{t}} = \alpha_T \cdot \Delta \mathrm{T} + \frac{q}{\mathrm{c} \cdot \rho} \tag{1}$$

where: $\alpha_T = \lambda/(c \cdot \rho)$ – diffusivity, c – specific heat, ρ – density, λ – thermal conductivity, ΔT = div(grad T) – Laplace temperature operator and q – thermal source $= c \cdot \rho \cdot \frac{\partial T_{ad}}{\partial t}$, defined as a function of adiabatic temperature rise (T_{ad}).

RCC thermal behaviour greatly depends on the hydration processes of cementitious materials (cement and fly-ash). Hence, an adequate hydration-heat model must be defined and used. The presented model uses the degree of reaction method, [5]. The degree of reaction, r(t), ranges from 0 to 1, and is defined as a ratio between the heat released from the beginning of the reaction to the specified time, t, and the total amount of heat released due to the hydration. The amount of released heat is a function of a temperature time-history, and is mostly influenced by the temperature dependant increment of hydration heat, $q_T(T)$, defined as:

$$q_T(T) = e^{\frac{-C_A(r,T)}{T+273}}, \text{ where } C_A(r,T) \text{ – Arhenius constant.} \tag{2}$$

The differential FEM matrix formulation of thermal-stress analysis yields [5]:

$$\mathbf{C} \cdot \dot{\mathbf{u}} + \mathbf{K} \cdot \mathbf{u} + \mathbf{f} = 0 \ , \tag{3}$$

where: **C**–damping matrix, **K**–stiffness matrix, **f**–vector of nodal loads, $\dot{\mathbf{u}}$ –vector of unknown velocities, and **u**–vector of unknown nodal displacements. If conductivity, specific heat, and/or boundary conditions are temperature dependant, the problem becomes nonlinear, and the equation system (3) has to be solved iteratively. The dam body and foundation rock have been discretized by solid brick twenty-node isoparametric elements. The element is based on the quadratic interpolation and Gaussian integration.

In the phased thermal-stress analysis, used in this research, computational results from the previous construction phase are stored, and used as an initial condition for the following phase. From one phase to another, new parts of the model may show up (and some become inactive), therefore the active elements have to be defined at the beginning of the each phase. Within the each phase, the computation is performed in a given number of time steps, defined according to the observed concrete placement schedule, [6], [7], [8].

3. Numerical model

The numerical model is developed using the Finite Element Method based on the *Diana* package, [5]. The FEM formulation of the heat conductivity equation (1) yields:

$$\mathbf{K} \cdot \mathbf{T} + \mathbf{C} \cdot \dot{\mathbf{T}} = \mathbf{Q} \ , \tag{4}$$

where: **K** – the thermal conductivity matrix, **C** – the capacity matrix, **Q** – the nodal discharge. Since a nonlinear thermal problem is considered (properties and/or the boundary conditions depend on time), the incremental-iterative method is used for solving eq. (4).

The 3D model is applied to the non-overflow monolith, of the Platanovryssi dam. This dam is the highest to date RCC dam in Europe, 95 m high, with the crest length and width of

280 m and 7 m. The dam is built using 30 cm thick layers, and is divided into 13 monoliths by vertical contraction joints.

The initial conditions are defined by the temperatures at the finite element nodes, obtained from the observed mixture temperatures of each layer. The temperature boundary conditions include a constant temperature at the outside rock and the time variable temperature at the faces, galleries, or at the current top layer (during the construction), defined according to the available in-situ measurements [4]. The displacement boundary conditions are prescribed at the outer surfaces of the foundation rock.

4. Results of thermal field computation

The time evolution of the 3D thermal field of the representative dam monolith is presented in Fig. 1 and Fig. 2. During the initial phase of the construction, a "*hot core*" has formed some 10 m above the foundation line. The core has been gradually cooling for the following four months. By the summer, the air temperature rises, causing formation of another hot core (Fig. 1). After the completion of the dam, and the filling of the reservoir, only one hot core remains, at the centre of the dam (Fig. 2).

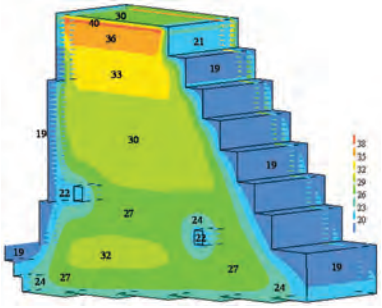

Figure 1. 3D Temperature field on 6.1.1996

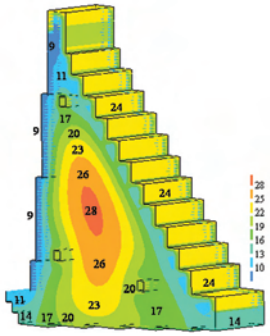

Figure 2. 3D Temperature field on 15.6.1999

5. Results of thermal-stress computation

The normal stresses in the dam-axes direction, σ_z, are considered. The stresses are primarily influenced by the temperature field, and to a less degree by the dead load, while the effect of other loads may be neglected, [8]. The tensile stresses are accepted to be positive, and the compressive stresses are negative.

Thermal-stress computation is performed for the 3 values of the monolith length: 16 m, 20 m, and 24 m. In this section, only the results for the 16 m monolith are presented.

At the Fig. 3, the stresses in the rock are equal to zero. Tensile stresses in the lower zone of the dam are less than 1.20 MPa (since the concrete have already reached its maximal temperature, and began to cool), while at the upper zone compressive stresses occur (as the temperature is still rising and the concrete is expanding). The stress concentration along the horizontal joints, between the successive layers are the consequence of the difference between the stiffness of the layers.

At the Fig. 4, 166 days after the commencement of concreting, the dam was 46 m high, with 153 RCC layers placed. The maximum tensile stress of 1.62 MPa occurred bellow the

ground level, at the vicinity of the upstream and downstream faces. The maximum compressive stress was -1.94 MPa.

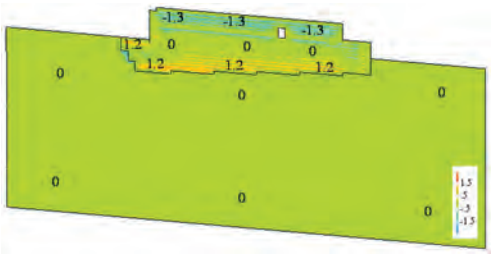

Figure 4. Middle plane stress-field, 1.4.1996

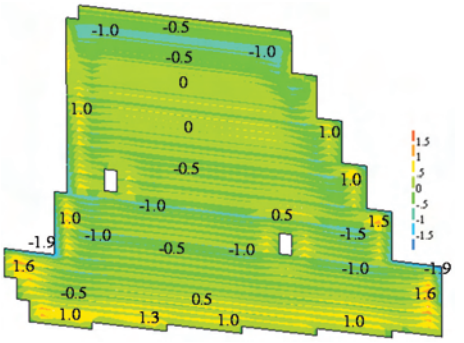

Figure 3. Middle plane stress-field, 9.1.1996

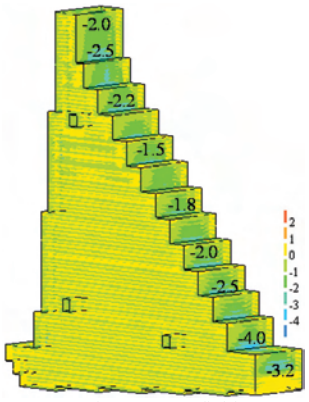

Figure 5. Surfaces Stress-field 1.9.1997

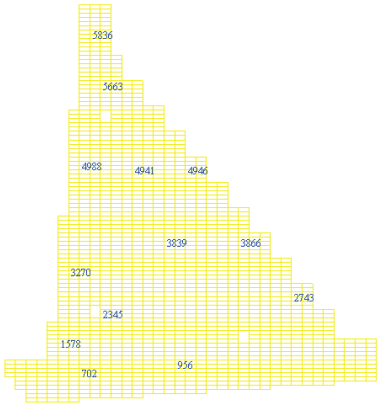

Figure 6. Characteristic elements at the middle plane

At Fig. 5, the dam was completed, but the filling of the reservoir has not begun. The maximum tensile stress of 2.21 MPa occurred in the middle plane, in the region of 10 m above the foundation line. The maximum compressive stress of -4.0 MPa occurred at the lower part of the dam, close to the downstream boundary.

The stress evolution in time is presented for the characteristic elements in the middle plain, Fig. 6. The results for the elements: 702, 2743, and 5836 are presented at Fig. 7.

One can observe that for all the elements, compressive stresses develop during the first 5 to 10 days after the placing, as a consequence of the hydration heat. The concrete tends to expand, and due to the restricted strains, the compressive stresses issue. When the concrete begin to cool, the shrinkage follows, and the tensile stresses result. The maximum tensile stresses depend on the temperature gradient, and the current stiffness of RCC.

The element 702 is within a massive structure, but relatively close to the upstream face, which influences the thermal-stress behaviour. After the initial compression, and tension phase, the stresses are mildly influenced by temperature boundary conditions. The element 2743 is strongly influenced by the downstream temperature boundary condition. Intensive

insulation causes high amplitude oscillations, together with the high tensile stresses (up to 0.8 MPa). The stress behaviour of element 5836 at the dam crest is governed by both, upstream and downstream boundary condition, with the less significant effect of insulation.

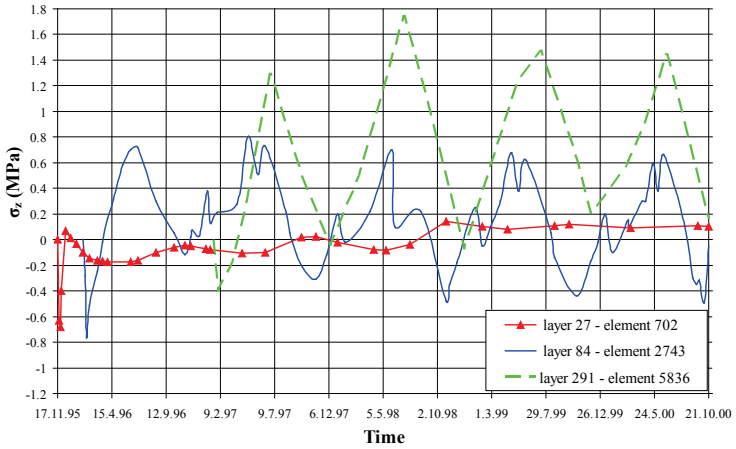

Figure 7. Stress evolution at the elements 702, 2743, and 5836

6. Evaluation of the transversal joint distance

The influence of temperature on the transversal joint distance is analysed, based on the results of the presented model, and the observed data. The length of the monolith of 16 m, 20 m, and 24 m is considered (models 3DL16, 3DL20, and 3DL24, respectively). At Fig. 8, the thermal stress evolution of the characteristic element in the middle plain is presented. One can observe that the stresses at the upstream face (the element 4988) follow the seasonal temperature oscillations. After the reservoir impounding, the stress oscillations dampen, due to the constant water temperature. The mean square deviation between 3DL24 and 3DL20 is negligible (0.07 MPa), comparing to the deviation of 0.16 MPa, between 3DL20 and 3DL16.

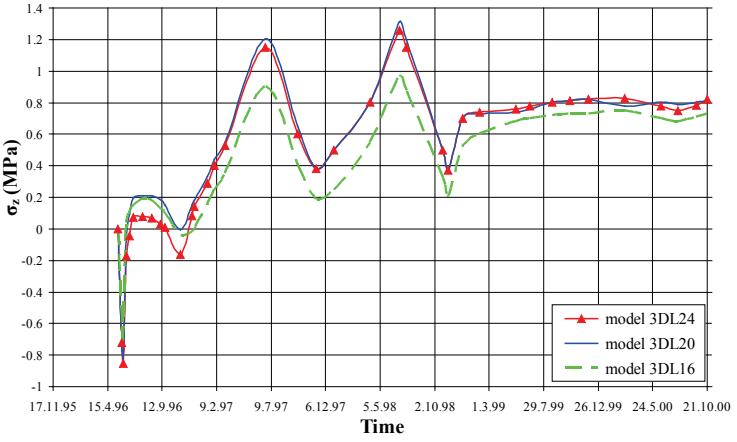

Figure 8. Stresses at element 4988 (layer No. 187), depending on the monolith length

Based on the maximum tensile stresses, their mean square deviation at characteristic elements, and the stress-field time evolution, it follows that the thermal stresses for RCC gravity dams depend on the monolith length. For the considered Platanovryssi dam, the mean square deviation of thermal stresses, between 3DL24 and 3DL20 is 0.11 MPa, and between 3DL20 and 3DL16 is 0.16 MPa. Increasing the monolith length from 20 m to 24 m, rises the maximal thermal stresses for about 0.33 MPa (12.2 %). Reducing the monolith length from 20 m to 16 m, decrease the maximal stresses for about 0.20 MPa (7.4 %).

Having in mind the computed maximal tensile stresses (depending on the monolith length), and the observed RCC tensile strength of 2.70 MPa [4], one may conclude that the maximal monolith length for the Platanovryssi dam should be 20 m. Bearing in mind that the constructed length of the particular monolith is 22 m, and with some cracking and leakage issuing at the downstream face (which implies exceeding of the tensile strength), it may be concluded that a somewhat shorter monolith should have been used.

7. Conclusions

- For the first time a comprehensive 3D numerical model for the phased thermal-stress analysis of the massive concrete structures has been developed, providing for a reliable evaluation of the transversal joint distance.
- Having in mind the maximum tensile stresses, their mean square deviation at characteristic elements, and the stress-field time evolution, it follows that the thermal stresses for RCC gravity dams depend on the transversal joint distance.
- The most important indicator of the thermal behaviour of RCC gravity dams, are the stresses in the direction of the dam axes.
- The shape of the diagram of the normal stresses time evolution, depends on the position in the middle plane, but it is almost independent on the monolith length
- It is not possible to formulate the universal suggestions for all RCC dams. Therefore, for each particular dam, the thermal-stress analyses should be performed to obtain the best estimate of the transversal joint distance.

Acknowledgement. This work was supported by the Ministry of Education and Science of the Republic of Serbia under project no. TR 37009 “Monitoring and Modeling of Rivers and Reservoirs – Physical, Chemical, Biological and Morphodynamic Parameters”.

References

[1] Crichton A, Benzenati I, Qiu T, and Williams J (1999), Kinta RCC Dam – Are Oversimplified Thermal-Structural Analysis Valid?, *Proceedings of Australian National Committee on Large Dams Conference*. Jindabyne, pp. 446-457.
[2] Aniskin N A (2006) Temperature regime of a gravity dam from rolled concrete, Power Technology and Engineering, vol. **40**, pp. 23-27.
[3] Malcolm Dunstan & Associates Consulting Engineers (1996), *Platanovryssi Hydroelectric Project, Review of the Properties of the Concretes in Platanovryssi Dam*, Devon, England.
[4] Public Power Corporation (2004), *Platanovryssi Hydroelectric Project, Measurement Results*, Athens, Greece.
[5] TNO Building and Construction Research (2002), *Diana User’s Manual*, Delft, The Netherlands.
[6] Kuzmanović V (2007) Thermal-stress analysis of roller compacted concrete dams (in Serbian). *PhD thesis*, Department of Civil Engineering, The University of Belgrade, Serbia.
[7] Kuzmanovic V, Savic Lj and Stefanakos J (2010), Long-term thermal analysis of RCC dams using 2D and 3D models, *Canadian Journal of Civil Engineering*, vol. **37**, pp. 600–610.
[8] Kuzmanovic V, Savic Lj and Mladenovic N (2013), Computation of Thermal-Stresses and Contraction Joint Distance of RCC Dams, *Journal of Thermal Stresses*, **36**, pp. 112–134.